




REGIONAL CLASS RESEARCH VESSEL

Model Test Report

PREPARED FOR: Department of the Navy Washington, DC		BY: Amy T. Gooden PROJECT ENGINEER	
  GLOSTEN 206-624-7850 www.glostent.com		CHECKED: William L. Moon, III PROJECT NAVAL ARCHITECT	
DOC: DI-010-05 REV: A FILE: 06059.11		APPROVED: Bruce L. Hutchison, P.E. PRINCIPAL-IN-CHARGE	
		DATE: 12 November 2008	

Revision History

Section	Rev	Description	Date	Approved
App. B	A	Final Report - Additional appendage documentation, photos of streamlines, comments and self-propulsion raw data	10/29/08	BLH
App. C	A	Final Report – Update of appendices and incorporation of final propeller results from the model basin (BSHC).	10/29/08	BLH
App. E	A	Final Report - Update of Figure 4.1	10/29/08	BLH
References	A	Changed Reference 1 to Rev A	11/6/08	BLH

References

1. Glosten/NBBB Item No. DI-010-02, Speed and Power Report, Rev A, November 2008

1 Objective

The following report gives the objective and results of the hull form optimization, wake-adapted propeller design, and the model testing.

2 Methodology/Results

In an effort to reduce hull resistance and bubble sweep-down over the swath mapping sonar array a hull optimization was carried out by Friendship Systems. The resulting optimized hull form had a 22% reduction in resistance, 55% increase in streamline distance to the free surface and a 50% reduction in wave-making resistance. The results of the hull optimization can be found in Appendix A.

In conjunction with the hull optimization, model tests for hull resistance, self-propulsion, detailed wake survey and propeller cavitation of the final design wake-adapted propeller were performed by the Bulgarian Ship Hydrodynamics Centre (BSHC), the results of which are discussed in detail in the speed and power report (Ref 1), Appendix B and Appendix D.

Terry Brockett was employed to design an optimized Ice Class D0 wake-adapted propeller, which is cavitation free in all operating conditions and at all speeds in the vessel's full displacement condition. The propeller design can be found in Appendix C and cavitation results can be seen in the speed and power report (Ref 1) and Appendix D.

Appendices

Appendix A – Friendship Systems Report, “Formal Hull Form Optimization of a RCRV”

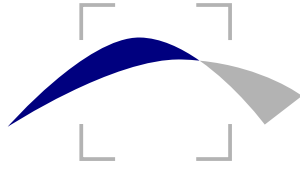
Appendix B – Bulgarian Ship Hydrodynamics Centre, “Hydrodynamic Model Tests of Regional Class Research Vessel – Powering Tests with Stock Propellers, Rev. 1”

Appendix C – Terry E. Brockett, PhD, “Design Summary: Powering Propeller Model Geometry for the Glosten RCRV Twin-Screw Vessel,” Final Draft

Appendix D - Bulgarian Ship Hydrodynamics Centre, “Hydrodynamic Model Tests of Regional Class Research Vessel – Powering Tests with Final Design Propellers, Rev. 0”

Appendix E - Bulgarian Ship Hydrodynamics Centre, “Hydrodynamic Model Tests of Regional Class Research Vessel – Cavitation Tests with Final Design Propeller, Rev. 1”

Appendix A Friendship Systems Report, “Formal
Hull Form Optimization of a RCRV”



FRIENDSHIP SYSTEMS

Formal Hull Form Optimization of a RCRV

for
The Glosten Associates, Inc.

FS-Report 118-15-01

Confidential

The information provided in this report is confidential.

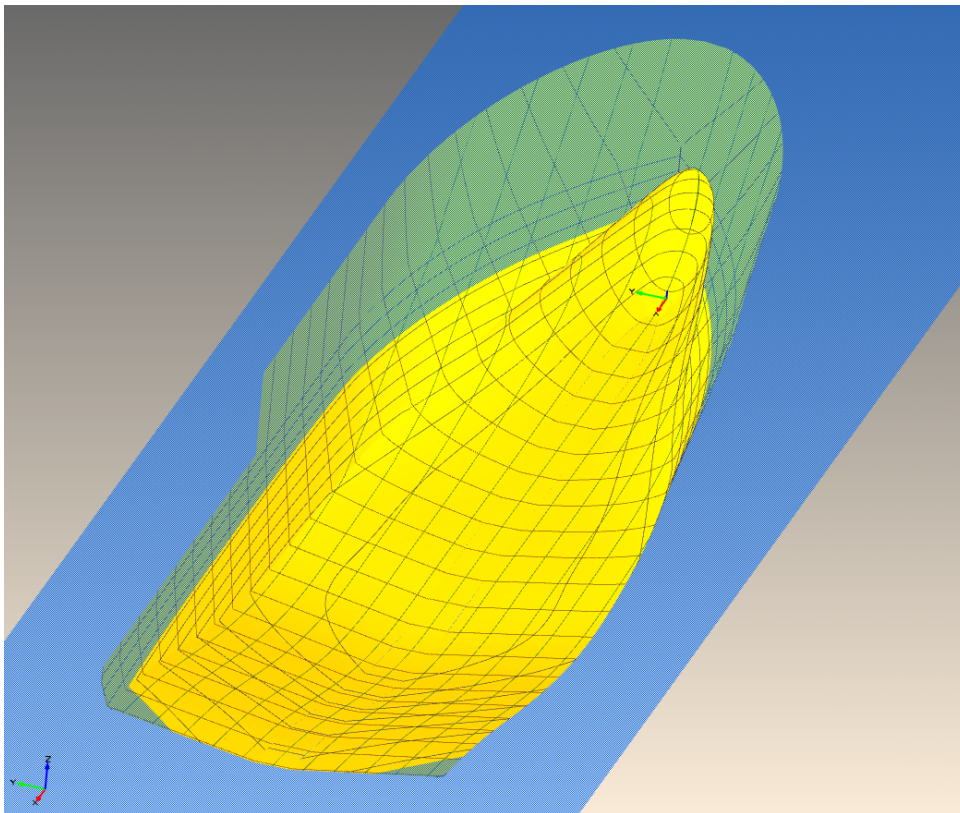
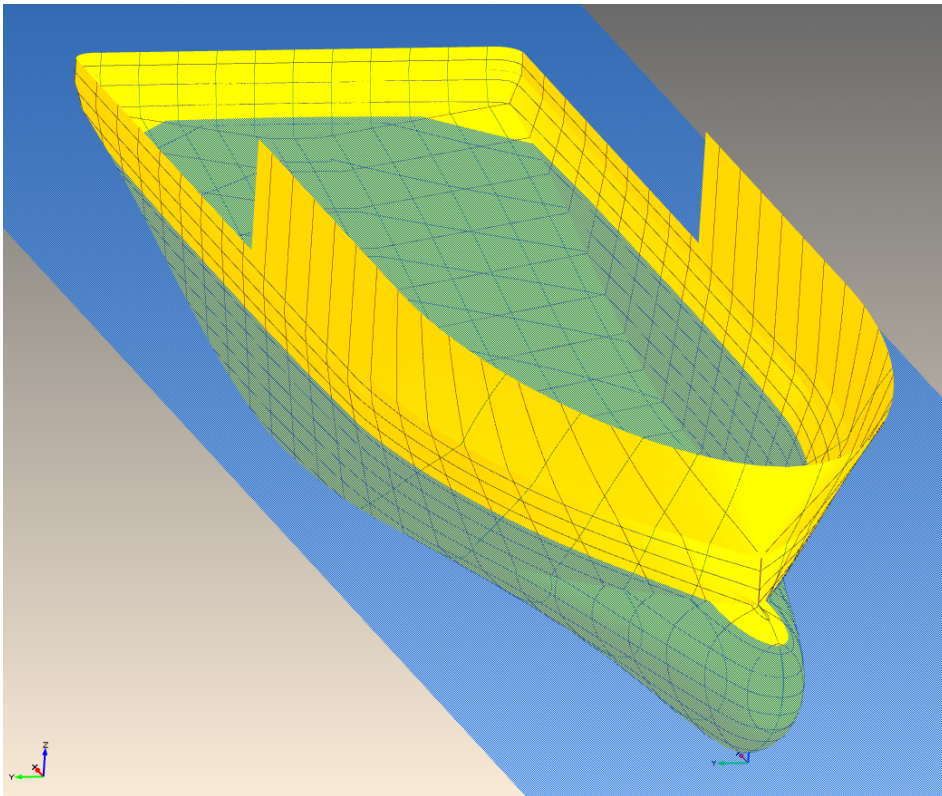


FIGURE 1: Render views of the optimized hull *TSearch_016/DES_0044mod2* generated within the FRIENDSHIP-Framework .

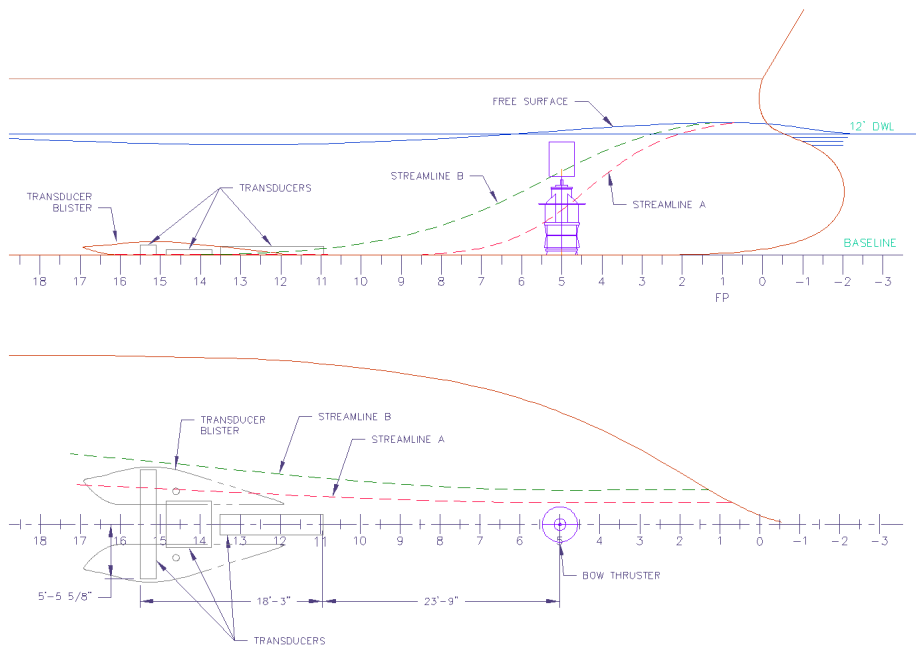


FIGURE 2: Arrangement plan of the swath mapping sonar transducer, courtesy of The Glosten Associates, Inc..

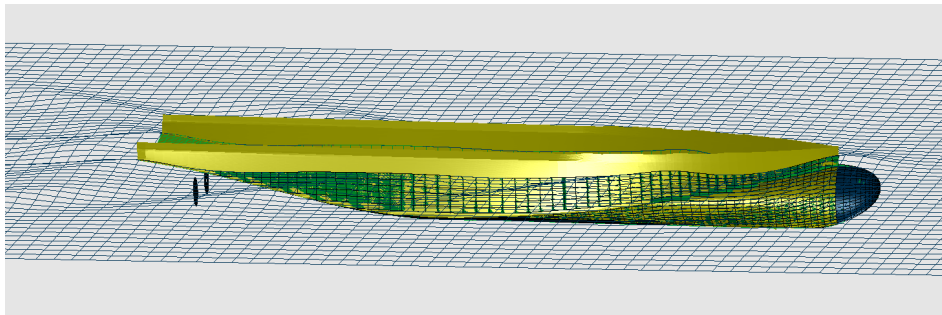


FIGURE 3: Optimized hull *TSearch_016/DES_0044mod2* at 10 kn computed by FS-Flow .

Overview

A hydrodynamic optimization of the *Regional Class Research Vessel* was conducted for The Glosten Associates, Inc. with the objectives of reducing both the performance at the service speed of 10 kn and to minimize the risk of bubble sweepdown from the upper bow edge to the so called swath mapping sonar transducer mounted at the keel at approx. $1/3 L_{PP}$ downstream of FP, compare figure 2. The optimization had to meet a set of important constraints. The main parameters of the *RCRV* are given in table 1. Figure 1 shows render views of the optimized hull *TSearch_016/DES_0044mod2*. Figure 2 gives the arrangement plan of the swath mapping sonar transducer figure 2 (courtesy of The Glosten Associates, Inc.).

The hull shape of the *RCRV* was modeled by by means of a specifically developed **FRIENDSHIP-Framework** parametric model. A set of form parameters which effectively control the hull geometry was assigned to be the leading free variables in the optimization.

On the performance side either the total resistance, the thrust power or the delivered power are potential measures to be applied as objective function. For the



number of designs. Figure 11 show the optimization history, exemplarily for run *TSearch_000*.

From the optimization database hull variant *TSearch_016/DES_0044* was finally selected as overall favorite design. At the end of the optimizations minor changes were made to the hull shape in order to accommodate additional fairness requirements. The respective modified design *TSearch_016/DES_0044mod2* was further analyzed and compared against its predecessor. As expected the hull modifications somewhat reduced the performance gains, however, only by a very small, negligible amount.

The *TSearch* databases are provided in the accompanying Excel spreadsheets *FS-118-15-RCRV_FinalTSMDatabase_filtered_071002.xls* and *FS-118-15-RCRV_NewTSMDatabase_filtered_071022.xls*.

6.3

Results

The percentage gains and changes of the optimized hull *TSearch_016/DES_0044mod2* compared to the baseline hull are summarized in table 2. Additional parameters for both hull variants are listed in table 1. All constraints were satisfied. Substantial gains were obtained by the optimization both in the *RCRV*'s performance and in minimizing the risk of bubble sweepdown to the sonar transducer. Moreover, the displacement could be increased at the same time by 5.8% compared to the baseline hull.

Figure 12 to figure 14 show render views of the optimized hull *TSearch_016/DES_0044mod2* generated within the *FRIENDSHIP-Framework*.

In figure 15, figure 16 and figure 17 the effective thrust computed by *FS-Flow*, the predicted delivered power and the bubble-sweepdown-criterium, respectively, are plotted against the speed range. Figure 15 and figure 16 indicate a decreasing gradient of the thrust and power consumption around 10 kn. If this can be verified by model tests the *RCRV* maybe operated even at speeds beyond 10 kn at a similar cost level. In conclusion it is recommended to operate the *RCRV* either up to 6 kn or at its service speed and possibly above. Whereas, persistent operation at the intermediate speed range around 7-9 kn should be avoided to reduce the risk of unfavorable wave train interferences.

TABLE 2: Predicted percentage gains and changes of the optimized hull *TSearch_016/DES_0044mod2* compared to the baseline hull.

Gains and changes due to optimization:			$\frac{\text{opt} - \text{base}}{\text{base}} \cdot 100$
Delivered power @ TDES and 10 kn	P_D	%	-22
Bubble-sweepdown-crit. @ TDES and 6 kn	z_{min}	%	+55
Thrust @ TDES and 10 kn	T	%	-19
Total resistance @ TDES and 10 kn	R_T	%	-19
Wave-making resist. @ TDES and 10 kn	R_{WP}	%	-53
Displ. volume (bare hull) @ TDES	∇	%	+5.8
Wetted surf. area (bare hull) @ TDES	S	%	+4.2
Transv. metacentric height @ TDES	\overline{GMT}	%	+281

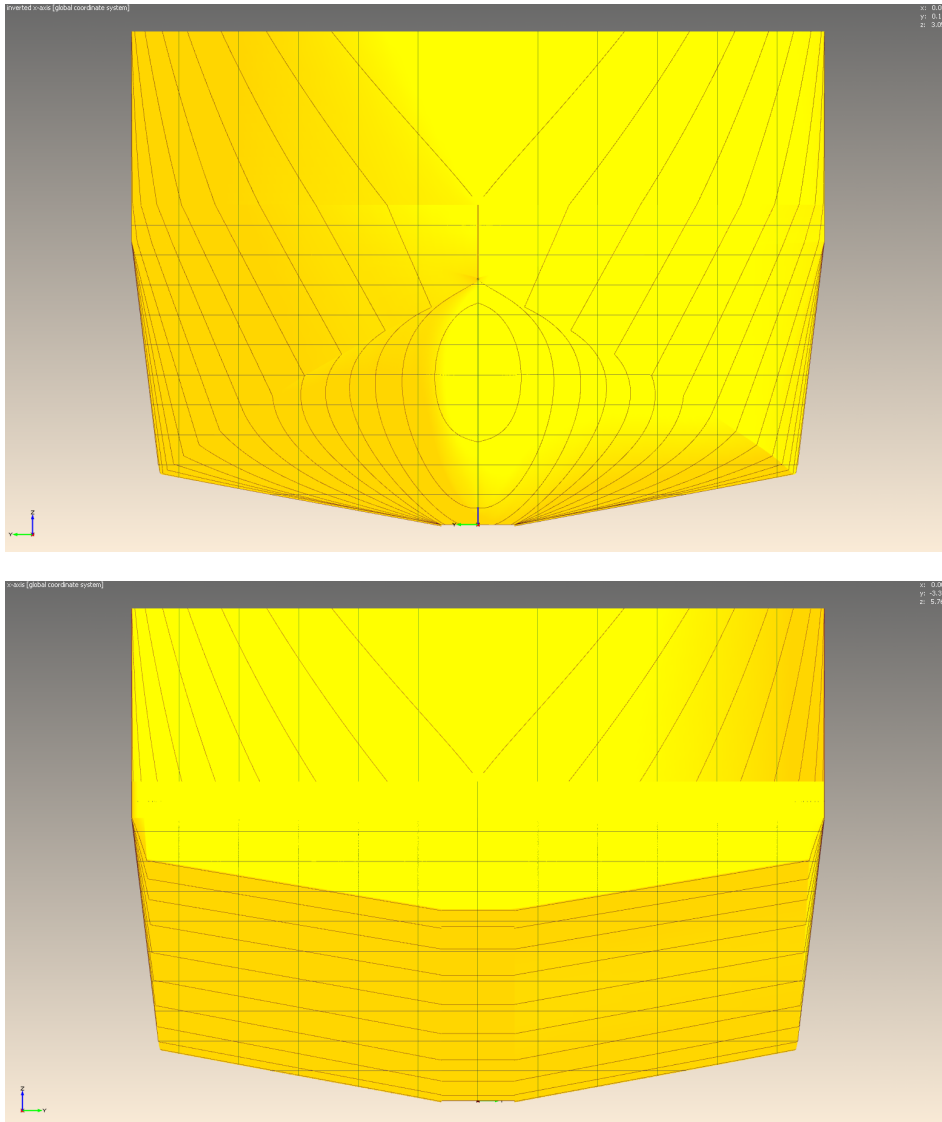


FIGURE 12: Bow and stern views of the optimized hull *TSearch_016/DES_0044mod2* generated within the FRIENDSHIP-Framework .

In view of figure 17 the risk of bubble-sweepdown to the sonar transducer seems to be relatively low even at speeds beyond the sonar speed. Figure 21 shows the track of the critical streamline for the baseline and the optimized hull.

The optimizations achieved a substantial reduction of the ship wave system at the service speed range. Figure 18 gives a comparison of the wave profile along the hulls and in figure 19 the longitudinal wave cuts at an offtrack position of $y/L_{PP} = 0.15$ are shown. The energy content in the wave systems was computed for the baseline and the optimized hull by conducting a longitudinal wave cut analysis which yields the wave pattern resistance, the latter being directly related to the area under the curves in figure 20. For details on the longitudinal wave cut analysis the reader is referred to Appendix B. A reduction of the single wave trains at the bow, at the fore and aft shoulder and at the stern as well as a favorable interference of the different wave trains along the hull lead to the reported substantial resistance reductions, compare figure 20. However, it should be noted that the significant reductions especially of the stern waves may be overstated by the potential

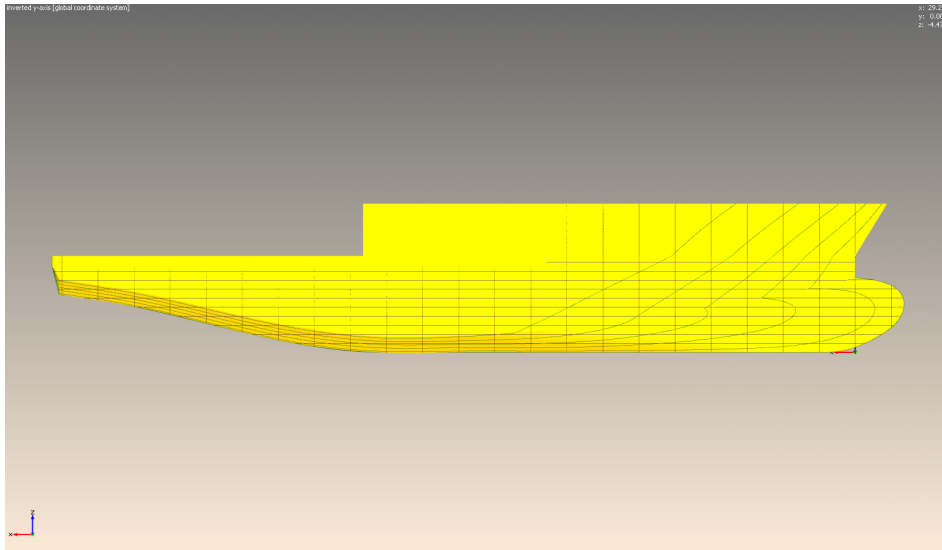


FIGURE 13: Side view of the optimized hull *TSearch_016/DES_0044mod2* generated within the FRIENDSHIP-Framework .

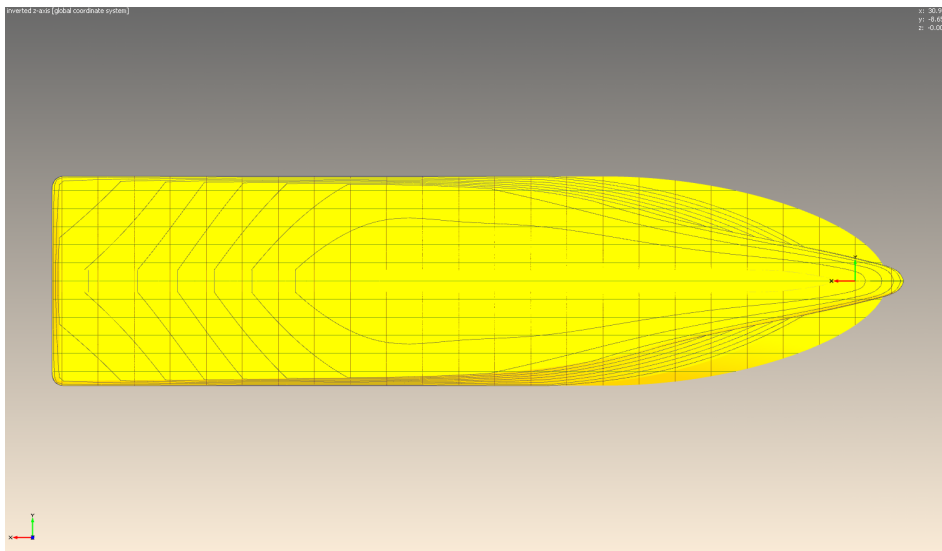


FIGURE 14: Bottom view of the optimized hull *TSearch_016/DES_0044mod2* generated within the FRIENDSHIP-Framework .

flow method and are not expected to be utilized to their full amount under real flow conditions.

From FS-Flow computations for the optimized hull with and without active propeller disk model a thrust deduction factor of $t = 0.146$ was derived.

According to the ITTC method the predicted viscous resistance component of *TSearch_016/DES_0044mod2* at service speed condition increased by abt. 3% compared to the baseline hull. This is in line with the increased wetted surface area of abt. 4% as a side effect of the hull modifications, especially, due to the increased breadth. On the other hand the predicted form factor $(1 + k)$ decreased slightly by 2.5% due to optimization. For a more detailed insight into the viscous flow phenomena accompanying viscous flow computations were conducted. De-

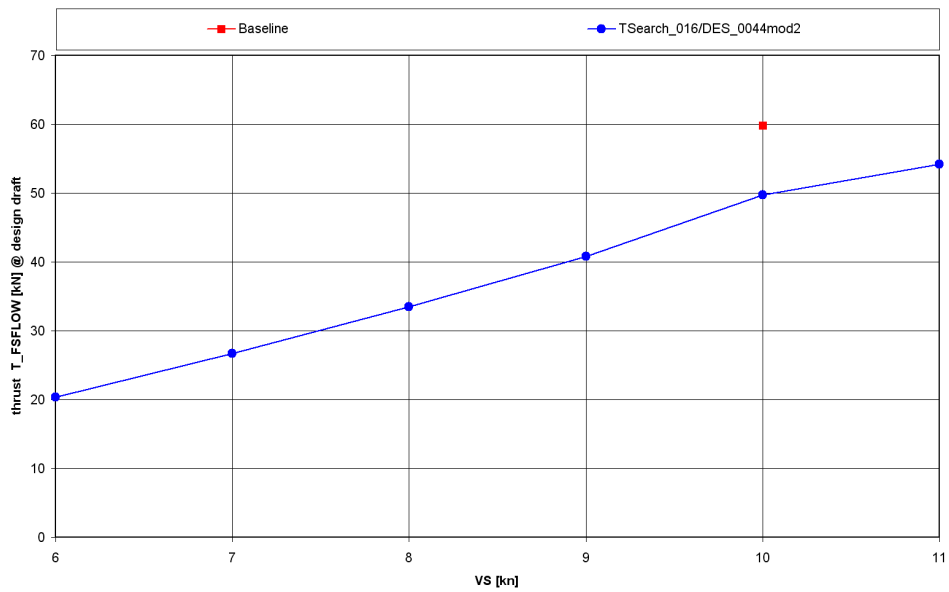


FIGURE 15: Comparison of the predicted propeller thrust @ design draft and 10 kn for the baseline and the optimized hull *TSearch_016/DES_0044mod2*.

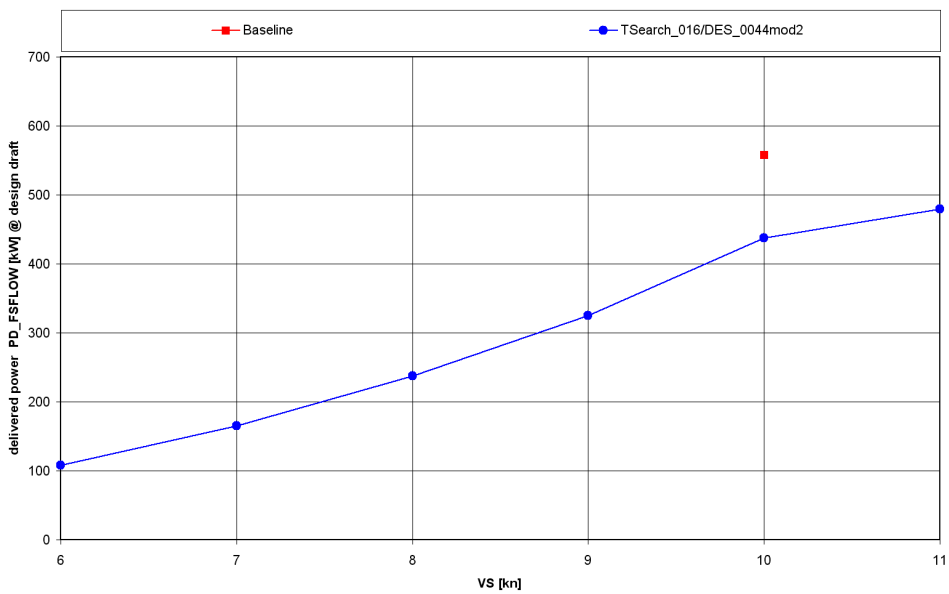


FIGURE 16: Comparison of the predicted delivered power @ design draft and 10 kn for the baseline and the optimized hull *TSearch_016/DES_0044mod2*.

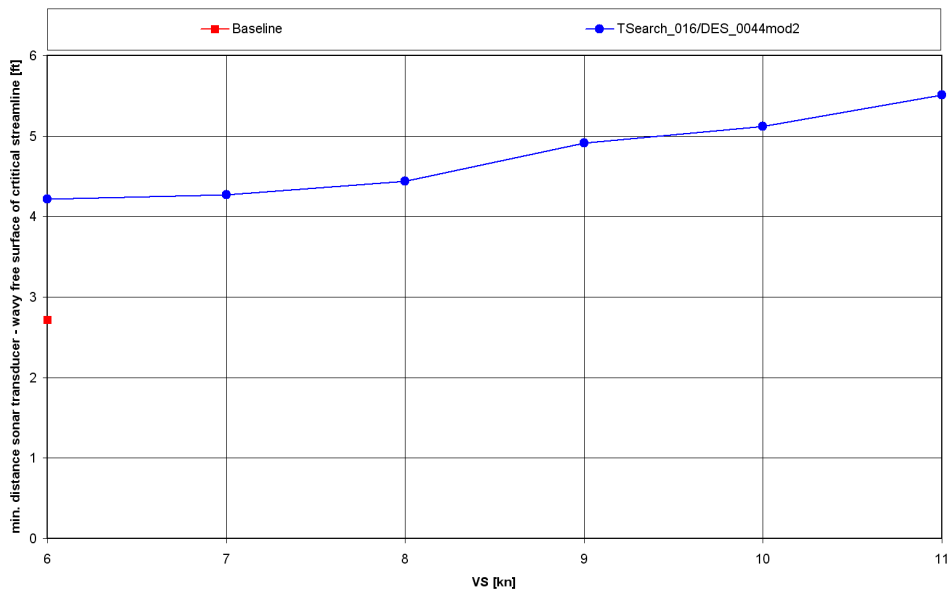


FIGURE 17: Comparison of the predicted bubble-sweepdown-criterion @ design draft and 6kn for the baseline and the optimized hull *TSearch_016/DES_0044mod2*.

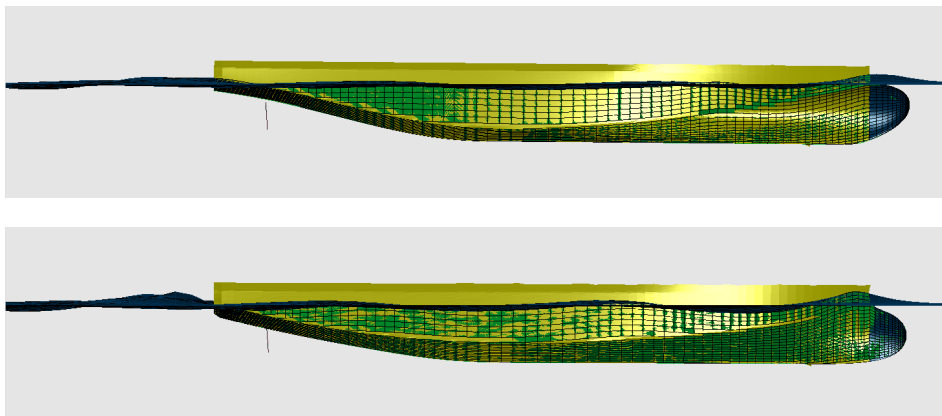


FIGURE 18: Wave profiles by FS-Flow @ design draft and 10 kn of the baseline (bottom) and the optimized hull *TSearch_016/DES_0044mod2* (top).

tails to the RANS computations are given in the accompanying PowerPoint presentation *FS-118-15-RCRV_XCHAP_071108.ppt*.

Figure 22 and Figure 23 shows the effective propeller wake and the vortex roll-up in the stern rise region which results from cross-flow over the lower aft knuckle line. Since the vortex roll-up is a source of extra drag rounding of the sharp knuckle in the stern region might be considered for the final hull construction. The propeller position is found to be suitable, however, the shaft inclination should be reduced as far as possible.



1.2 Principal model data

Ship model

Hull model No. : M0397

Model scale : 9.144

Particulars	Symbol/Dim		RCRV	Model
Length between perpendiculars	L_{PP}	[m]	43.891	4.800
Length on waterline	L_{WL}	[m]	46.342	5.068
Moulded beam OA	B_{OA}	[m]	11.582	1.267
Moulded beam WL	B_{WL}	[m]	11.326	1.238
Draft at FP	T_F	[m]	3.658	0.400
Draft at AP	T_A	[m]	3.658	0.400
Displacement volume at design load, bare hull	∇	[m ³]	1024	1.339
Block coefficient *	C_B	[-]	0.563	0.563
Longitudinal C.B. rel. to Lpp ** (bare hull)	LCB	[m]	-0.307	-0.034
Wetted surface area, bare hull	S	[m ²]	612.96	7.331

Remarks: *) refer to LPP
**) positive ahead of midship section

Appendages: Bilge keels, skeg, transducer fairing, shaft struts, propeller shafts, rudders
Total wetted surface area 0.724 m²

Turbulence stimulators: 1.7 mm trip wire at station 1

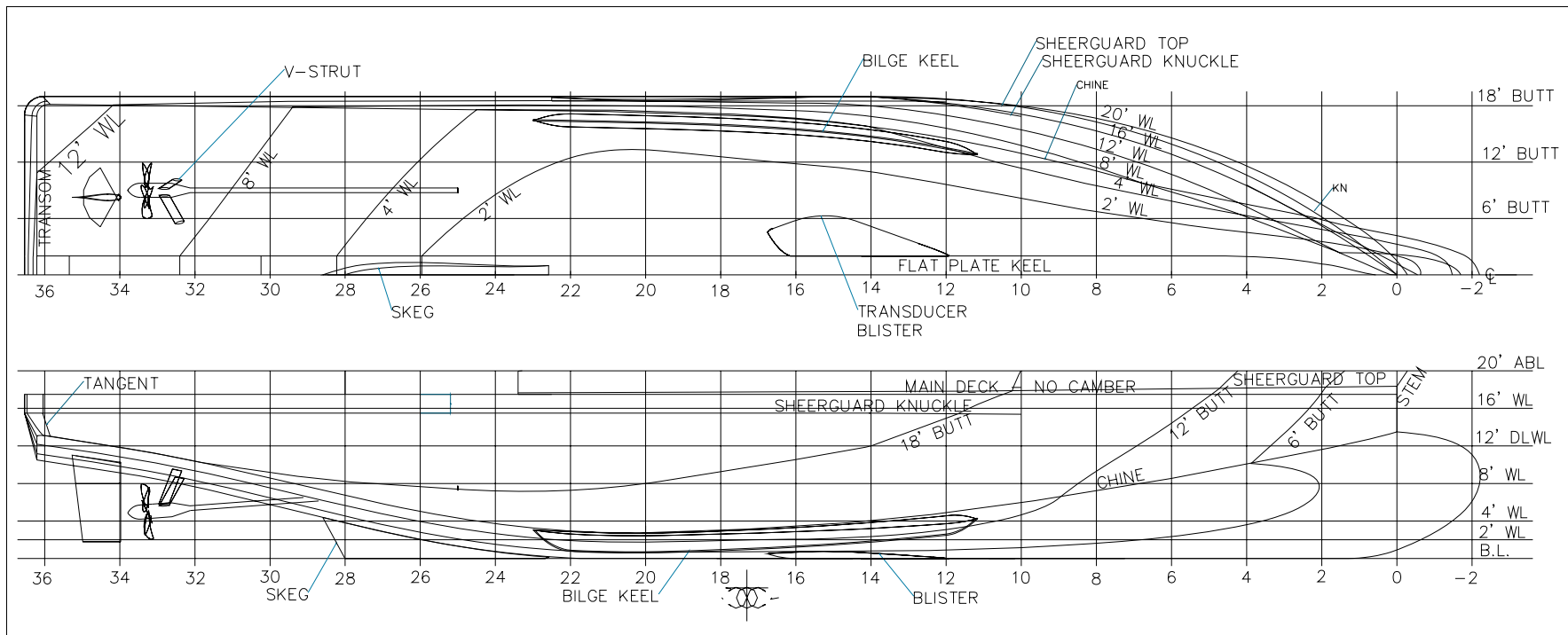


Fig. 1.2.1 M 0397 – body lines drawing

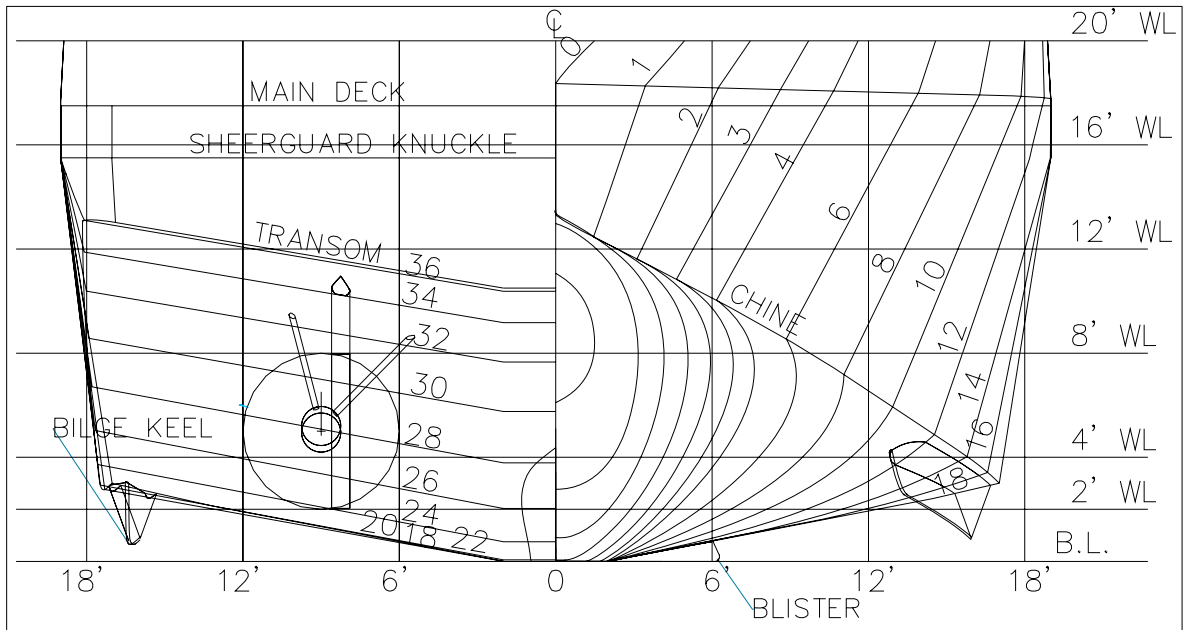


Fig. 1.2.2 M 0397 – body lines drawing

Appendages

The ship model was outfitted with the following appendages:

- Two bilge keels made of PVC (Fig. 1.2.3);
- A skeg made of “Abachi” wood (Fig. 1.2.4);
- A transducer fairing (blister) made of “Abachi” wood (Fig. 1.2.5);
- Two shaft V – struts made of steel (Fig. 1.2.6);
- Two rudder-rudder strut assemblies fabricated of PVC (Fig. 1.2.7).



Photo 1.2.1 Stock propeller models

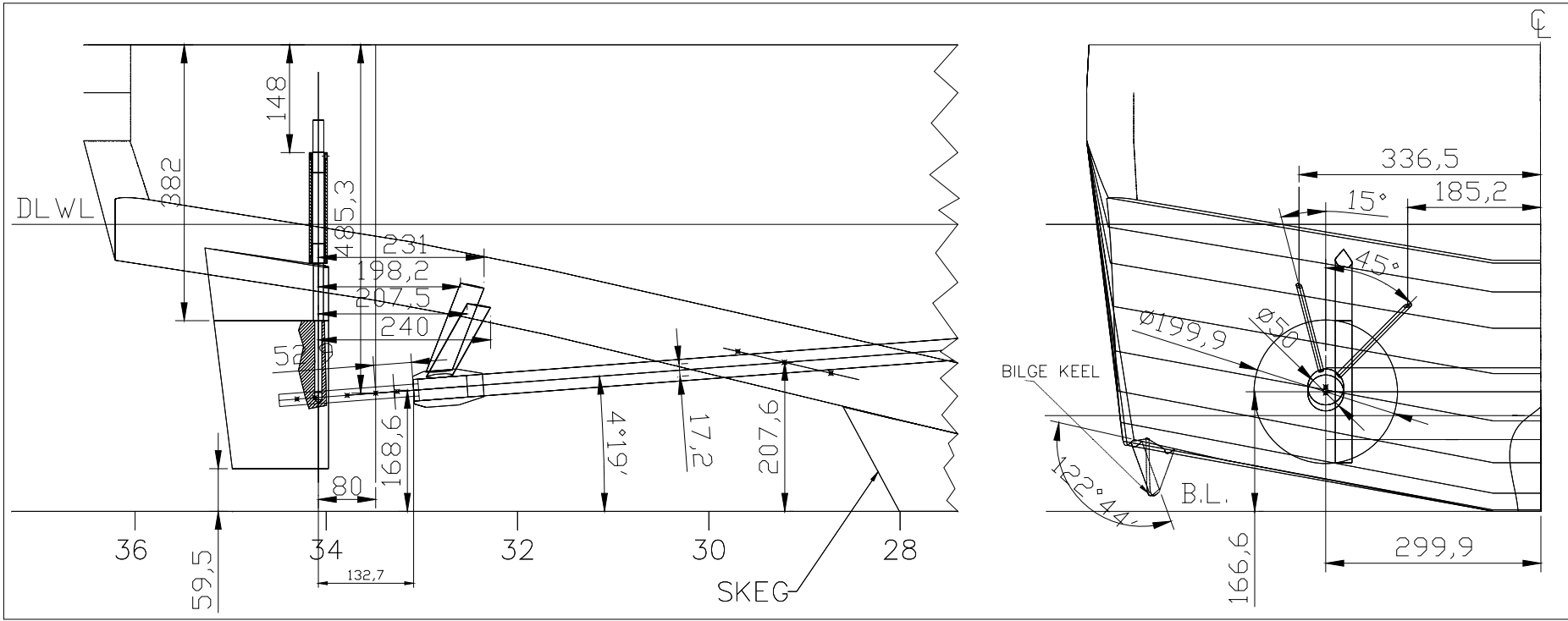


Fig. 1.2.8 Propeller-rudder arrangement





1.3 Test program

The model tests were carried out in accordance with the summary Table 1.3.1.

Table 1.3.1 Table of performed model tests

Test type	Model No.	Condition	Speed in knots	Description in Appendix
Resistance test – bare hull	M0397	Design draft	6 - 12	1
Resistance test – appended	M0397	Design draft	6 - 12	1
Propeller open water test (incl. thruster unit)	P0193/P0197	-	-	2
Self-propulsion tests	M0397 P0193/P0197	Design draft	6 - 12	3
Wake survey	M0397	Design draft	10	5
Streamline paint test	M0397	Design draft	10	-



2. POWERING TESTS RESULTS

2.1 Resistance tests results

Resistance tests have been carried out with bare hull and appended hull of the vessel in order to estimate the appendage drag.

The tests have covered the speed range of 6 to 12 knots. Low speed runs have been done for estimating the form factor using the Prohaska's procedure.

Positive values of draft variation correspond to sinkage of the hull, i.e. the hull moves downwards.

The full scale resistance has been predicted by the extrapolation procedure (Appendix 1) using an estimate of the appendage drag coefficient derived from the difference between the appended and bare hull model resistance in the range of the highest Reynolds numbers tested. However, this report provides all data necessary to apply the ITTC'78 procedure directly to the appended hull test results, e.g. wetted area of appendages, form-factor of the appended hull of the vessel.

Photos of the flow around the hull at speeds 6 – 12 knots are included in this report. More detailed visualization with photos and video are contained in a DVD accompanying the report.

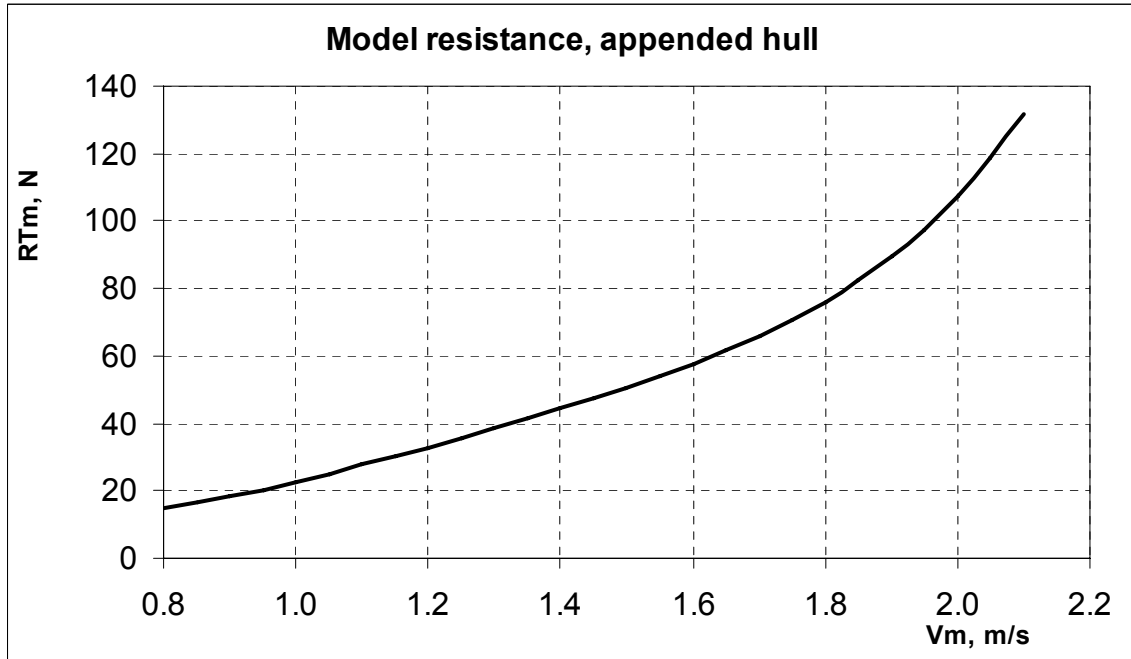
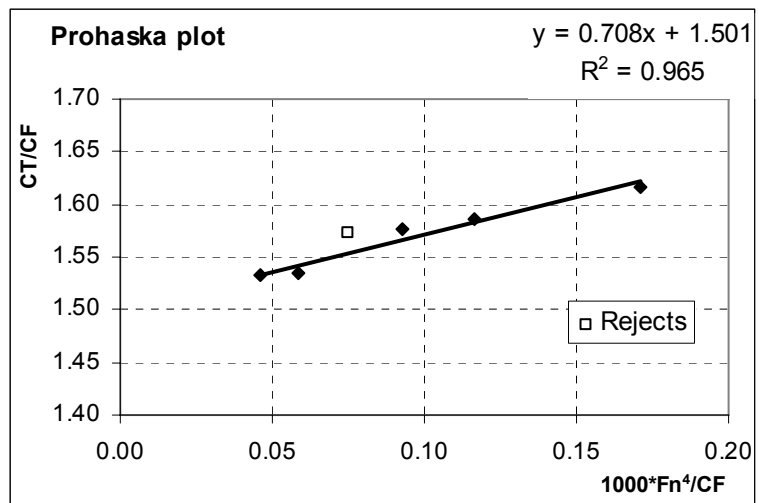


Fig. 2.1.3. Ship model resistance, Appended hull, Design draft

Measurements used for form-factor estimation	
Vm	RTm
m/s	kgf
0.8060	14.79
0.8520	16.39
0.9040	18.68
0.9520	20.56
1.0040	22.79
1.1010	27.45

(Shaded points are rejected)



Form-factor evaluated from low-speed runs: $1 + k = 1.501$

This form-factor is not used in the full-scale prediction according to the procedure used but is evaluated and presented here for possible alternative analyses.

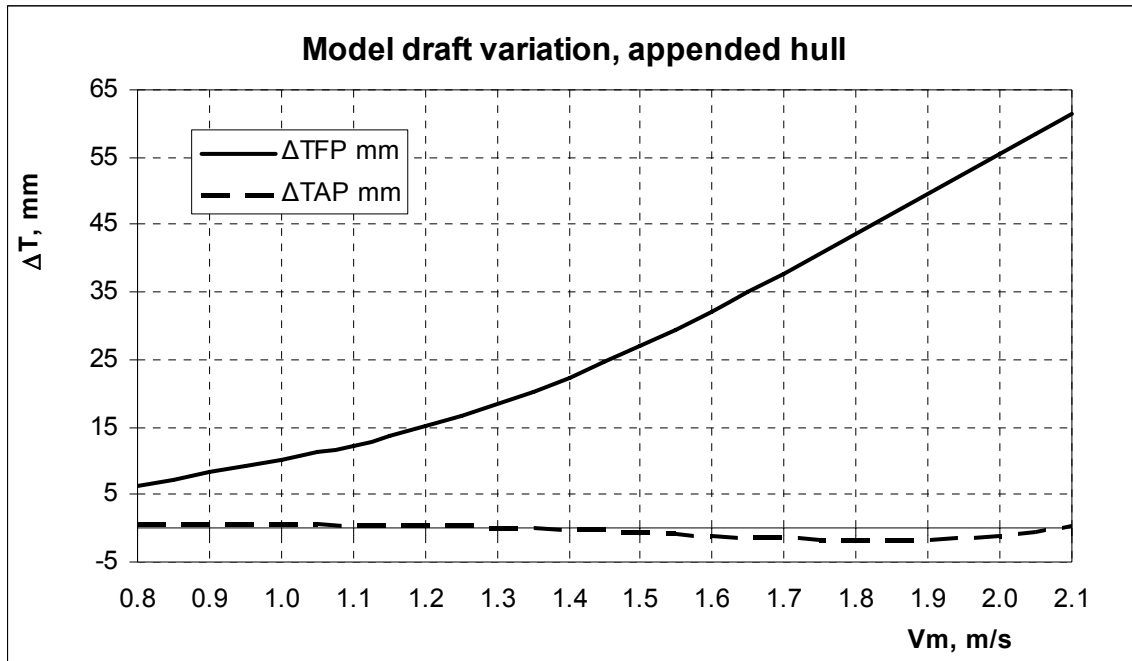


Fig. 2.1.4. Draft variation, Appended hull, Design draft



4.1 Wave pattern

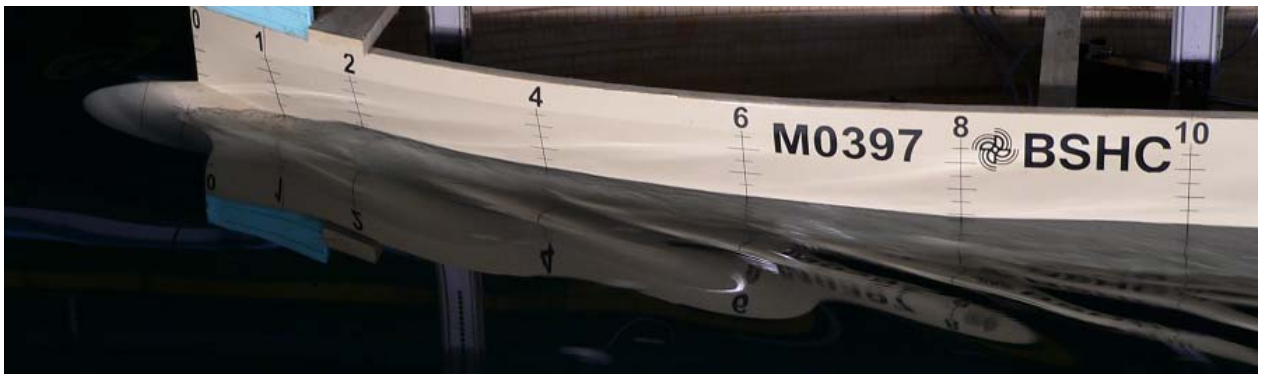


Photo 4.1.1 Wave pattern, Design draft, $V_S = 6$ knots



Photo 4.1.5 Wave pattern, Design draft, $V_S = 10$ knots

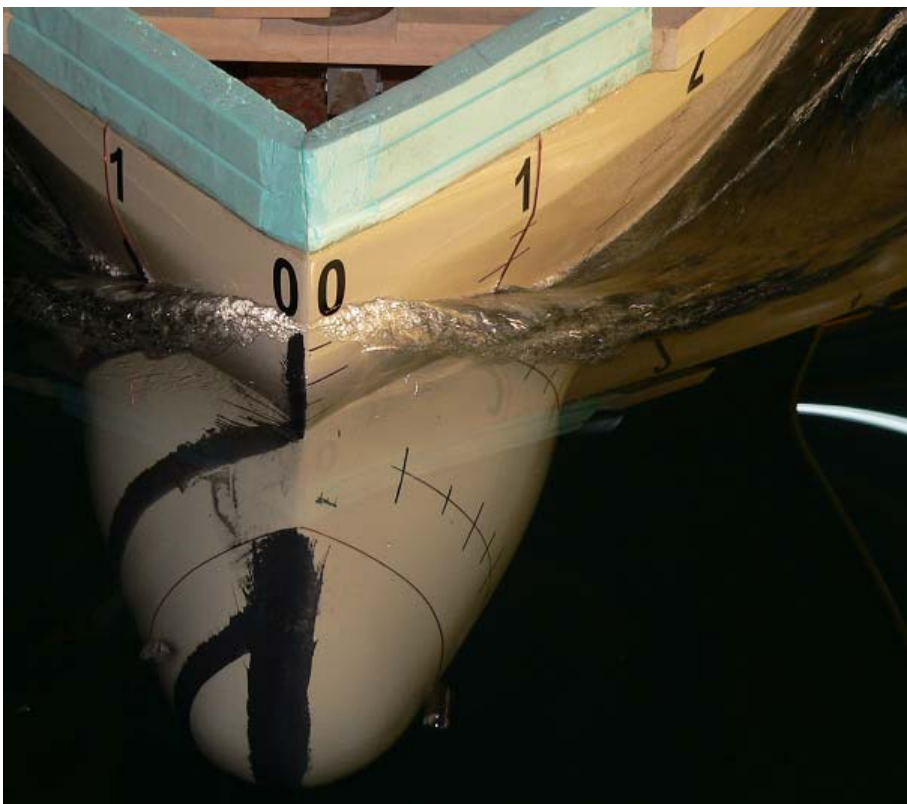
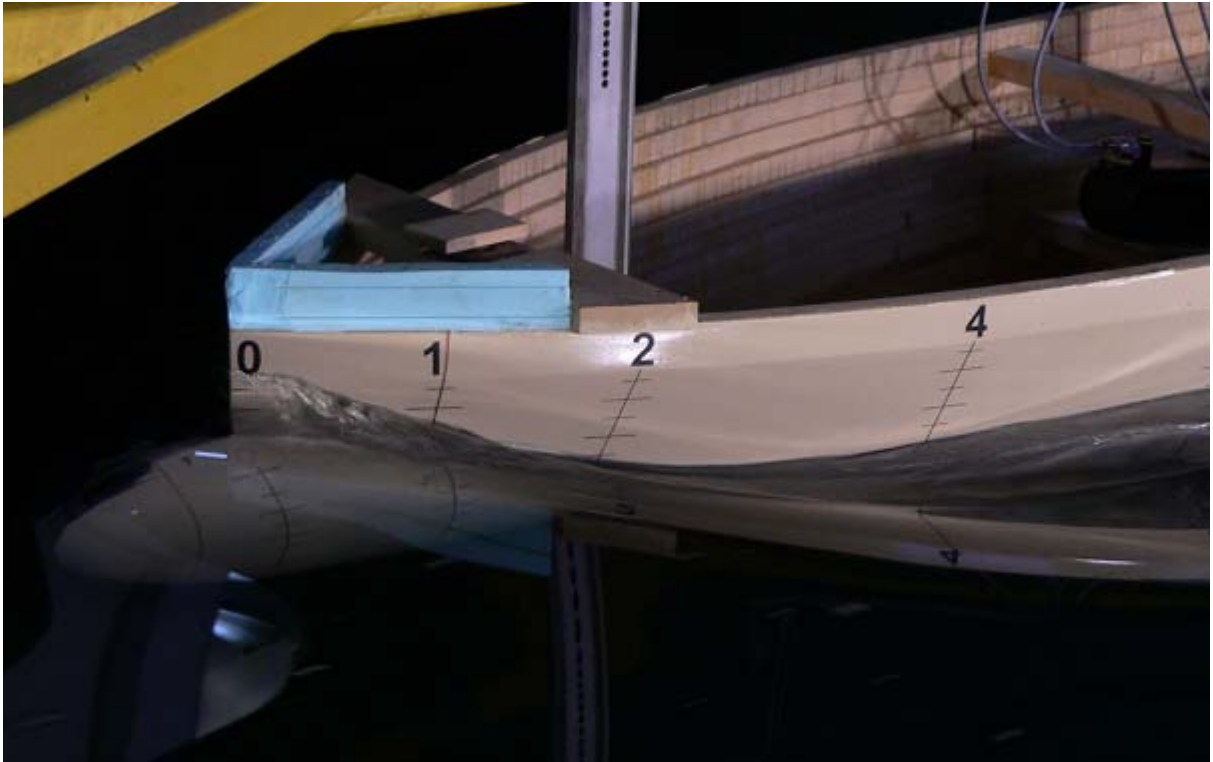


Photo 4.1.6 Wave pattern, Design draft, $V_S = 10$ knots



Photo 4.1.8 Wave pattern, Design draft, $V_S = 12$ knots

Final-Design Undertaking

ABS Ice-Class Rules were applied for the final design, resulting in wide blades and an EAR of greater than 0.6. This large EAR resulted in a preference for reduced rpm and the 200 rpm motor series was selected by Glosten. Design candidates were iterated until the TVi and powering reached an acceptable compromise. An overall propulsive coefficient of 0.63 together with a top speed of 11.3 knots (almost a knot and a half reduced from the exploratory design) and estimated inception speed for tip-vortex cavitation of 12.9 knots (not including a possible 3-knot margin for statistical variations) is achieved for the final design. The lifting-line output for this design is given in Appendix B. As already noted, the blades are massive compared to structural requirements for conventional hydrodynamic loads at top power. Blade-surface cavitation was estimated for several radial stations using the wake survey and design information. It was found that a thickness ratio (T/C) of 0.08 was reasonable near the tip and that the ABS Ice Rules provided adequate thickness at the inner radii. In order to produce low fluctuating loads, 5 blades and a skewed blade-reference line are specified. The skew is what is sometimes called balanced and allows for a sharp gradient at outboard blade radii while keeping the ABS-definition of skew modest (by the ABS definition, the blade is skewed about 25 degrees). The final pitch and camber are determined with a lifting-surface design code (Brockett, 1981). Two sketches of the final design rotor are shown in Figure 3 and a table of design geometry is included below. The data are believed fair and accurate to at least 1 in the third significant figure. As is evident in the sketch, the blade total rake (axial mid-chord position) is zero. This is selected to keep the axial position of the blade edges within the plane of the hub edges so the blade can be laid flat on either hub face without any special stand.

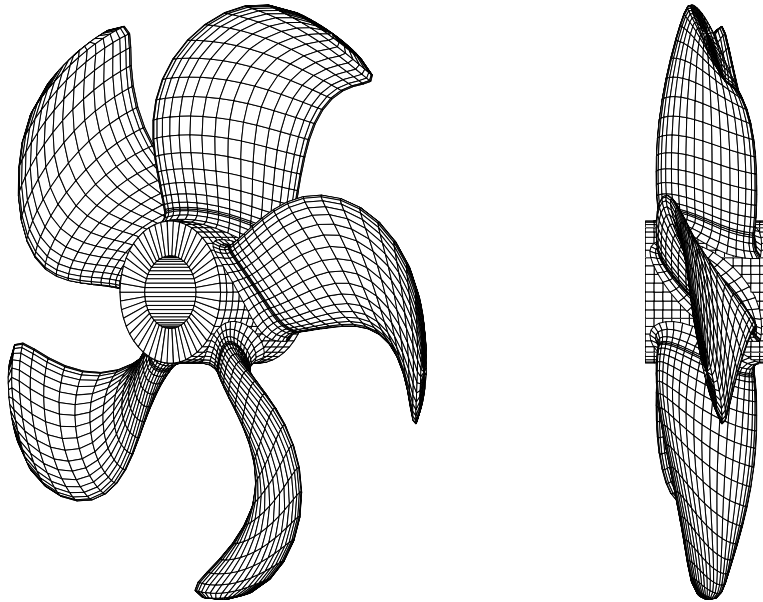


Figure 3: Final-Design RCRV Rotor - Starboard Propeller

The geometry definitions employed for the RCRV design are illustrated in Figure 2. Figure 4 displays the final geometry variables for the RCRV propeller.

also be performed. Preliminary scaling calculations indicate that the prototype blades should be cavitation-free at 11.3 knots.

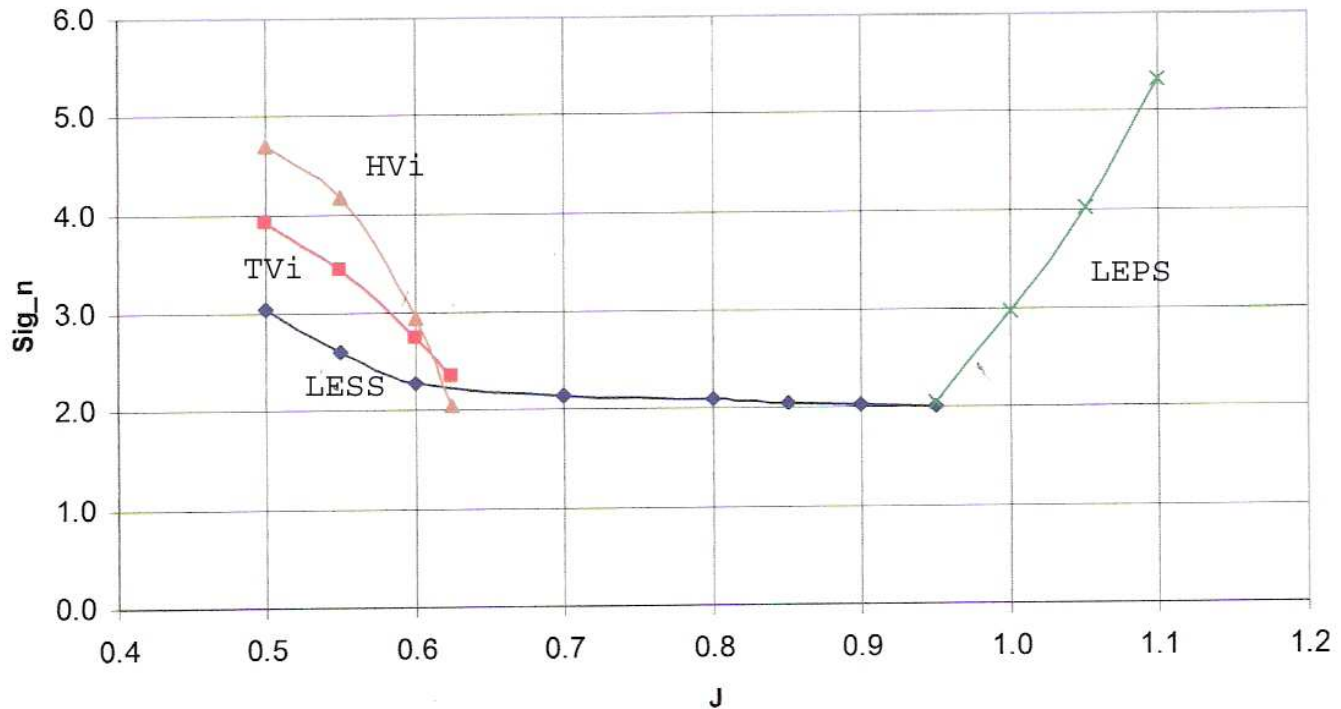


Figure 7: Preliminary Cavitation Tests, Shaft Inclination 12 Degrees

SUMMARY

A propeller design suitable for application on the Glosten Associates RCRV hullform is described. Lifting-line and lifting-surface numerical models of the flow about the blades have been employed to develop a geometry suitable to meet powering and cavitation goals. The blade outline and section thickness have been set by ABS Ice-Class Rules D0. A finite-element structural model has also been employed to confirm structural integrity due to hydrodynamic loads at maximum ahead speed. Preliminary data from model-scale tests of the propeller suggest the propeller meets design goals for loads and cavitation performance.

Delay of tip-vortex cavitation remains a challenge in design. A review of approaches to delay of tip-vortex cavitation inception suggests that tip unloading is robust - but produces degraded efficiency - while local geometry modifications remain risky. Additional effort to describe the state of the art for TVi is recommended.



Photo 1.2.1 Final design propeller models for powering tests



Photo 1.2.2 Propeller-rudder arrangement



TEST CONDITION

$N_s = 200.0$ rpm, $V_s = 11.3$ knots

$\sigma_n = 5.366$, $K_T = 0.192$



Fig. 3.2 $\varphi=0^\circ$



Fig. 3.3 $\varphi=60^\circ$

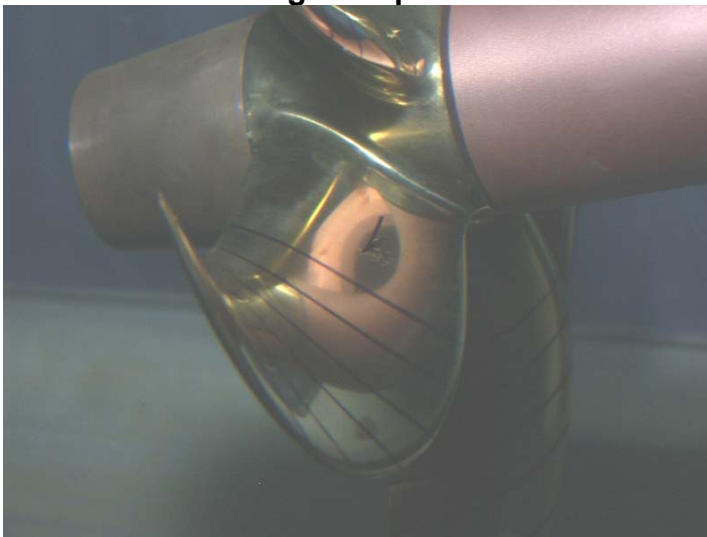


Fig. 3.4 $\varphi=120^\circ$

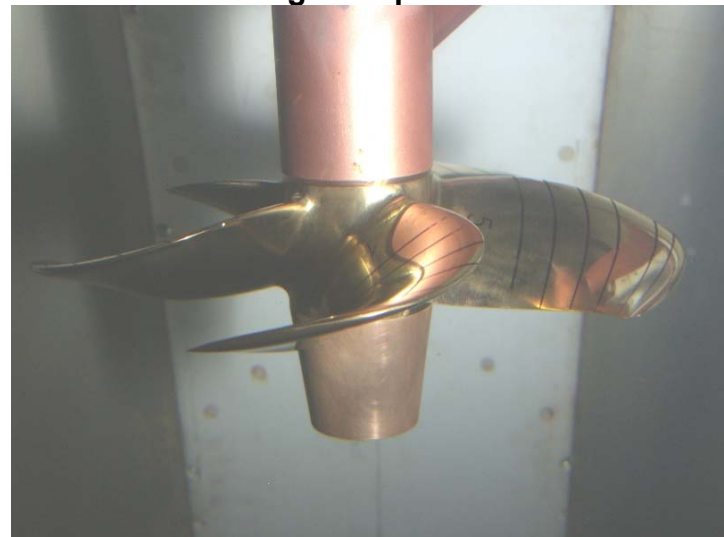


Fig. 3.5 $\varphi=180^\circ$

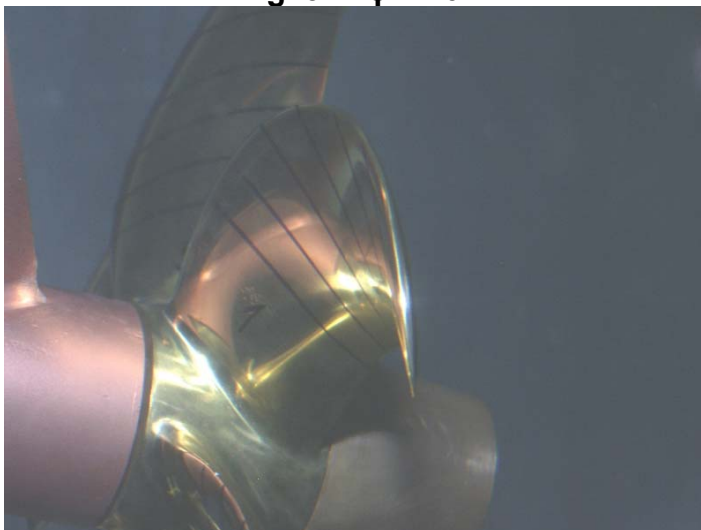


Fig. 3.6 $\varphi=300^\circ$

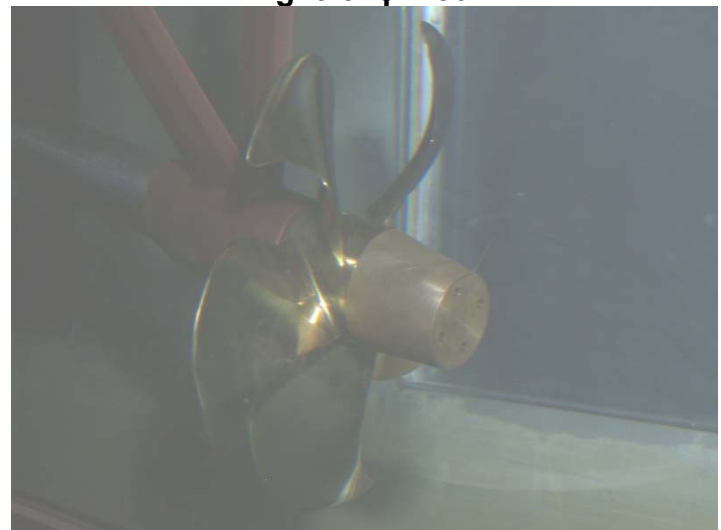


Fig. 3.7 Pressure side



4. CAVITATION INCEPTION TEST

According to ITTC recommended procedure this experiment consists of plotting observed cavitation points in a diagram of cavitation number (σ_n) versus advance coefficient (J). Points for the same type of cavitation are connected to determine inception boundaries of each form of cavitation.

The cavitation number is calculated on the basis of propeller revolutions. The propeller model has been rotated at 25 rps providing $Rn=10^6$.

The inception of four types of cavitation has been observed during the tests: Tip Vortex, Hub Vortex, Suction Side Sheet and Pressure Side. The results are shown on tables 4.1, 4.2, 4.3, 4.4 and fig.4.1.

Table 4.1. Suction side, sheet and cloud cavitation

J_s	n, rps	ΔH_{st} , mmHg*	σ_n
0.500	25.0	-283.7	3.054
0.550	25.0	-359.2	2.612
0.600	25.0	-416.5	2.276
0.700	25.0	-440.0	2.138
0.800	25.0	-447.0	2.097
0.850	25.0	-453.0	2.062
0.900	25.0	-458.5	2.030
0.950	25.0	-460.5	2.018

Table 4.2. Tip vortex cavitation

J_s	n, rps	ΔH_{st} , mmHg*	σ_n
0.500	25.0	-134.7	3.926
0.550	25.0	-219.0	3.433
0.600	25.0	-337.0	2.742
0.625	25.0	-402.7	2.357

Table 4.3. Hub vortex cavitation

J_s	n, rps	ΔH_{st} , mmHg*	σ_n
0.500	25.0	0.0	4.715
0.550	25.0	-90.0	4.188
0.600	25.0	-298.9	2.965
0.625	25.0	-455.0	2.051



Table 4.4. Pressure side cavitation

J_s	n, rps	ΔH_{st} , mmHg*	σ_n
0.950	25.0	-455.0	2.051
1.000	25.0	-296.0	2.982
1.050	25.0	-121.0	4.007
1.100	25.0	105.0	5.330

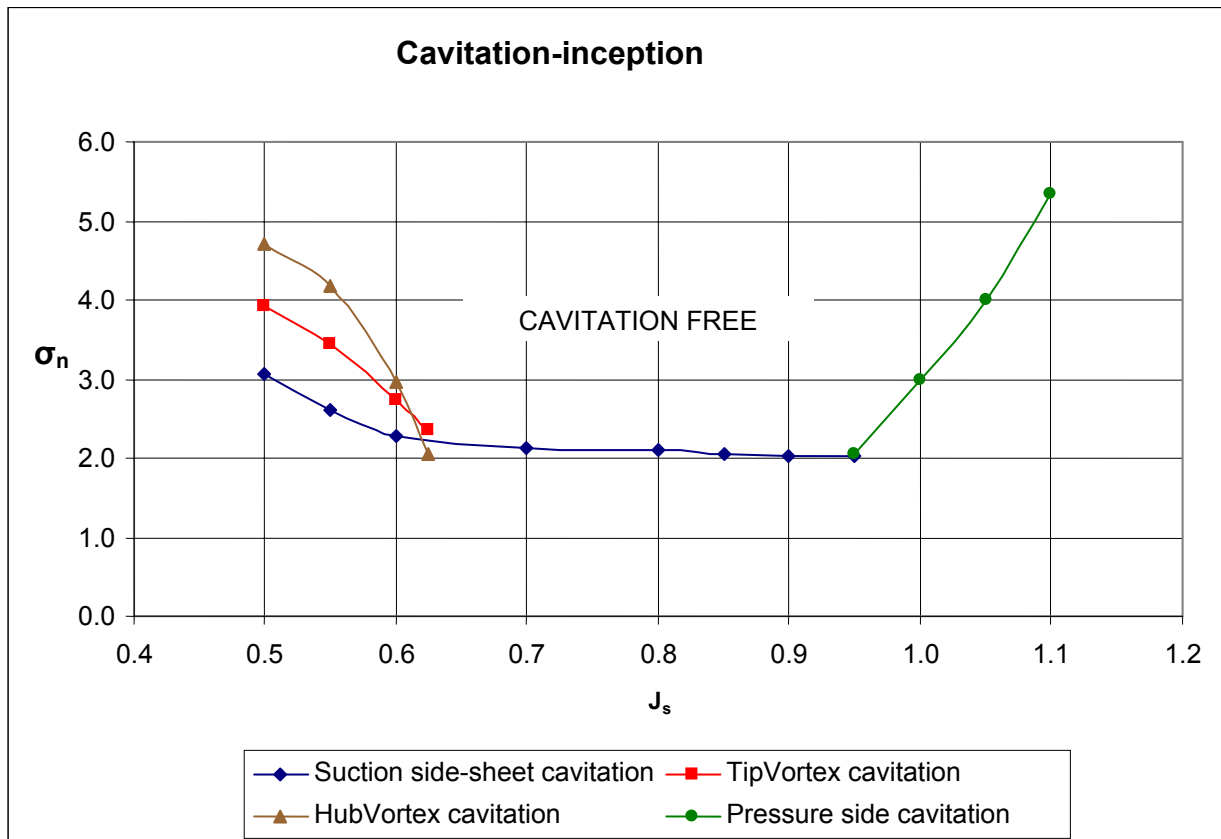


Fig. 4.1 Cavitation-inception Diagram

The performed observation of cavitation inception on propeller model P0633, operating behind the dummy shaft bracket, has shown the following:

1. At $J < 0.6$ and $\sigma_n < 4.8$ thin and stable hub vortex and tip vortex cavitation, a sheet cavitation initiating near leading edge at $r/R = 0.9 \div 1.0$ and a temporarily unstable sheet cavitation, transformed occasionally in cloud cavitation, in the region $r/R = 0.8 \div 0.5$ are observed (fig. 4.2 and fig. 4.3).
2. At $J > 0.6$ hub vortex and tip vortex cavitation are not observed (fig. 4.4 ÷ fig. 4.6).
3. A temporarily unstable sheet cavitation, transformed occasionally in cloud cavitation in the region $r/R = 0.8 \div 0.5$, is observed in the range $J = 0.62 \div 1.05$ at $\sigma_n < 2.2$ (fig. 4.4 ÷ fig. 4.6).
4. At $J > 0.95$ pressure side cavitation is also observed (fig. 4.7).
5. The portion of Cavitation-inception Diagram (fig. 4.1) located between "hub vortex cavitation", "Suction side-sheet cavitation" ($J > 0.63$) and "Pressure side cavitation" curves represents **cavitation free performance**.



Fig. 4.2 J=0.5 suction side



Fig. 4.3 J=0.5 suction side

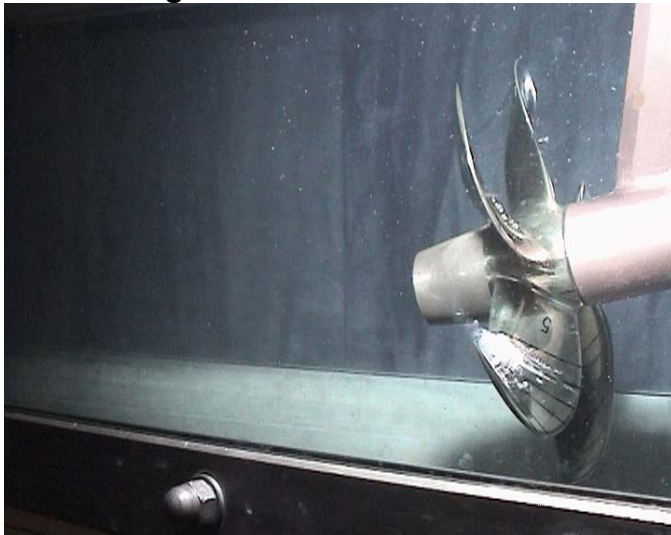


Fig. 4.4 J=0.7 suction side



Fig. 4.5 J=0.7 suction side



Fig. 4.6 J=1.0 suction side



Fig. 4.7 J=1.0 pressure side